Supporting Information

FeS_2 Nanoparticles in S-Doped Carbon: Ageing Effects on Performance as a Supercapacitor Electrode

Sirine Zallouz [1,2], Bénédicte Réty [1,2,3], Jean-Marc Le Meins [1,2], Mame Youssou Ndiaye [1,2], Philippe Fioux [1,2] and Camélia Matei Ghimbeu [1,2,3,*]

[1] *Institut de Science des Matériaux de Mulhouse (IS2M), CNRS UMR 7361, Université de Haute-Alsace, F-68100 Mulhouse, France*

[2] *Université de Strasbourg, F-67081 Strasbourg, France*

[3] *Réseau sur le Stockage Electrochimique de l'Energie (RS2E), FR CNRS 3459, 80039 Amiens Cedex, France*

* *Correspondence: camelia.ghimbeu@uha.fr ; Tel.: + 33 (0) 3 89 60 87 43*

Details for the XRD composition study:

The semi-quantitative (SQ) analysis is meaningful only if all the phases have been identified. It is performed on the basis of the pattern's relative heights and I/Icor values (when the reference standard Icor is Corundum). By definition $(I/Icor)_\delta$ is the ratio of the integrated intensities for CuKα radiation of the strongest line ($I_{rel} = 100$) of the phase δ to the strongest line of corundum for a 1:1 mixture by weight. This ratio (I/Icor) is read within the phase pattern of phase δ and is systematically present for patterns provided by the Crystallography Data Base (COD),[1] which is not systematic for PDF (Powder Diffraction File) files from ICDD (International Centre for Diffraction Data). Moreover, the I/Icor values for patterns calculated from the crystal structure are generally more reliable than the measured ones available in some PDF. For our study, the SQ analysis is based on the following hypothesis: all phases are crystalline and detected, which means that the software assumes that their sum is 100%.

This simple procedure is quick, easy, and convenient, but suffers as well from several drawbacks as described in detail in SI. Therefore, the objective here is to follow-up the evolution in time of the compositions within a multiphase mixture. The obtained raw values of the percentage of mass have no meaning other than for comparative purposes.

- the visual adjustment of the Y-scale values of each pattern: the relative height of a pattern may not match the measured scan (ie: in case of overlapping or preferred orientation),

- the peak height is proportional to the net area, which is true only if the peak broadening is similar for all the compounds of interest,

- the accuracy of the I/Icor value,

- the inhomogeneity of mixing.

Among all these drawbacks, the worst ones remain strong preferential orientation (texture) and overlapping, this is why we had to adapt and chose specific reflexion (ie: not the strongest one mandatory) for our phases to lead the study. The selected reflexions are less affected by this problem (but not exempt from), ie: generally non-orientation-dependent reflexions / limited overlapping. Once chosen, these reflexions were then systematically kept for the whole study. Therefore, in light of these many limitations, it is important to keep in mind that the results proposed here remain a semi-quatitative approach and have no value taken out of context. A Rietveld refinement should have given "real" quantitative analysis, but could not lead on such

complex mixtures sometimes with unequal crystalline quality, numerous phases and remain biased in the case of strong preferred orientation, even with tools like modified March's function.

Details on TGA analysis

TGA under air was conducted for all materials until 900 °C. The stages occurring during C/FeS_2 oxidation with temperature are:

1) Carbon matrix combustion, associated to mass loss due to CO_x gas release, and small amounts of H_2S, NO_x coming from doping.
2) FeS_2 oxidation according to Equation (S1). This leads to an increase of the mass due to the Fe_2O_3 formation, but also to a slight decrease of the mass due to the SO_2 release.

$$4\,FeS_2 + 11\,O_2 \rightarrow 2\,Fe_2O_3 + 8\,SO_2 \quad (S\,1)$$

An XRD on the resulting powder after TGA was performed and confirmed the Fe2O3 phase formation (Figure S5, SI). Based on the TGA residue amount, an estimation of FeS2 % in the different composites was conducted using equation (S1).

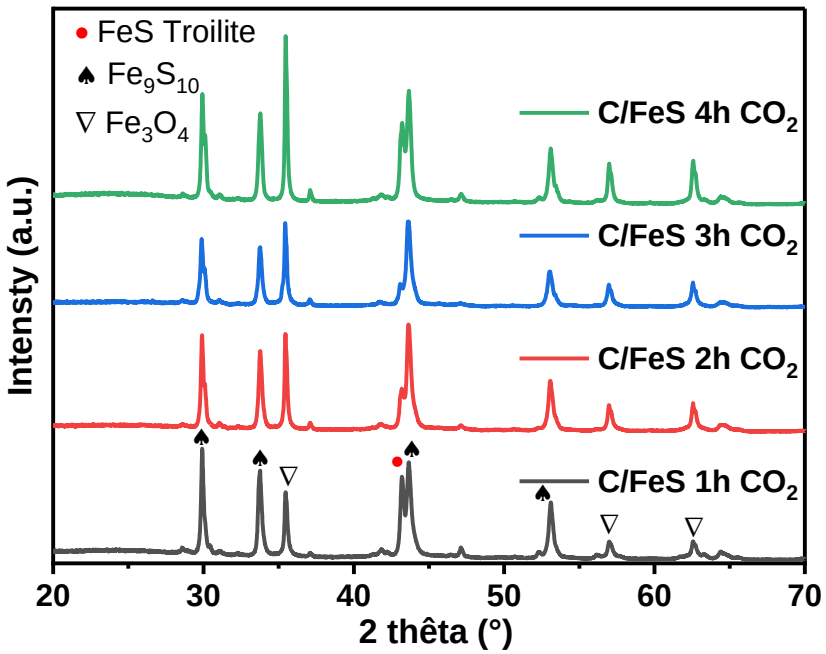

Figure S 1: XRD diffractograms of C/FeS composites after activation at different periods

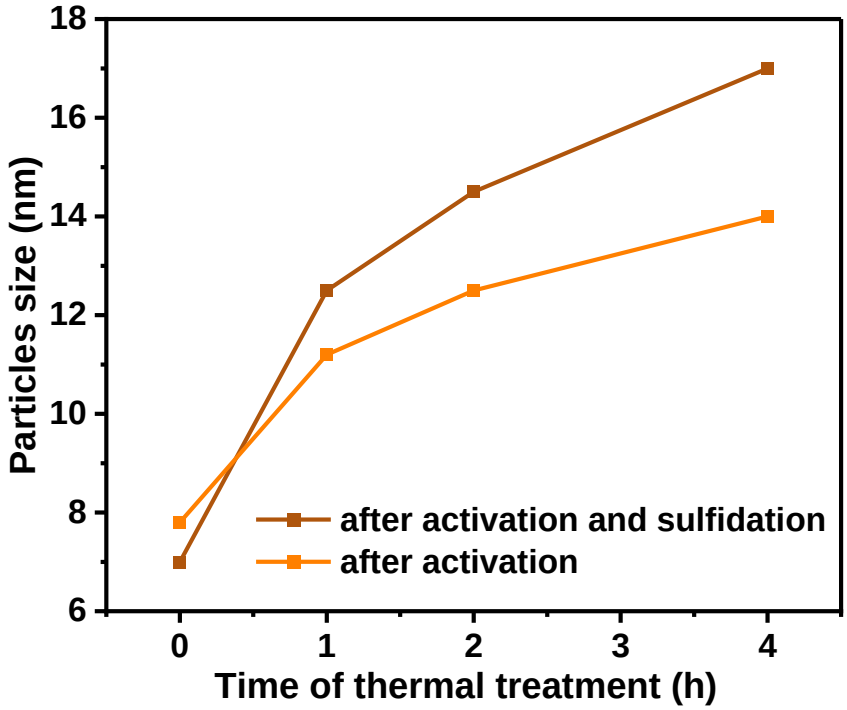

Figure S 2: Particle size evolution after activation (C/FeS) and after activation and sulfidation (C/FeS_2).

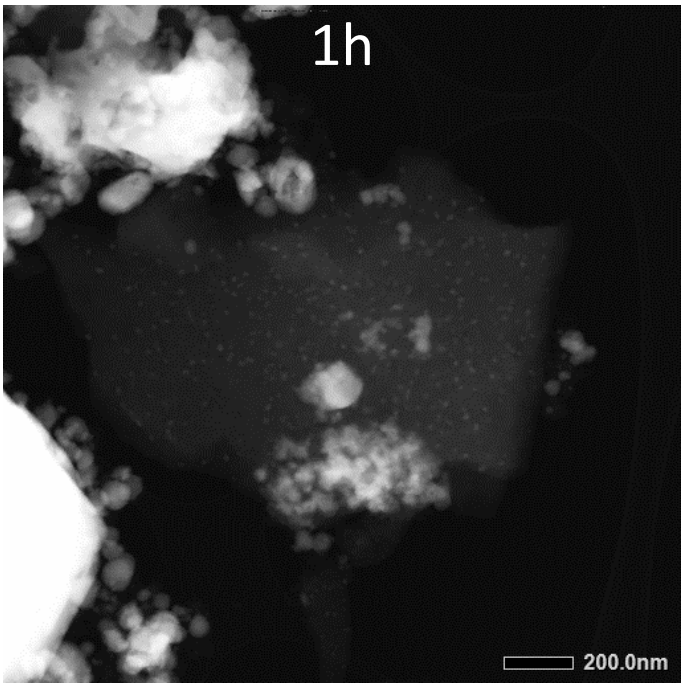

Figure S 3: STEM images for C/FeS_2 A 1h showing some agglomerated areas of FeS_2 particles.

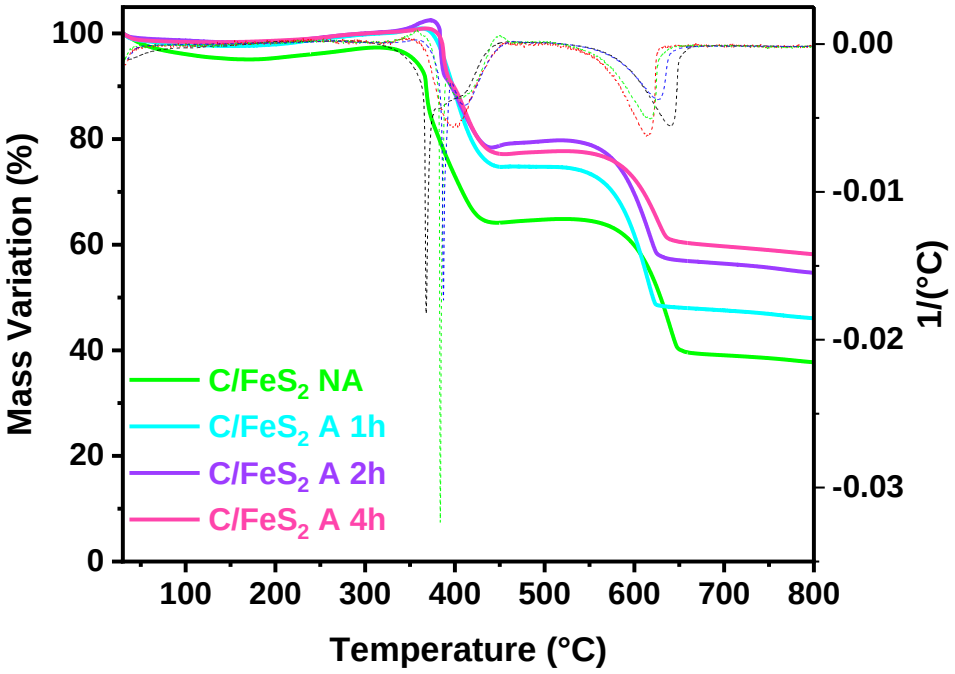

Figure S 4: TGA and DTG under air from 30 to 900 °C for C/FeS_2 composites.

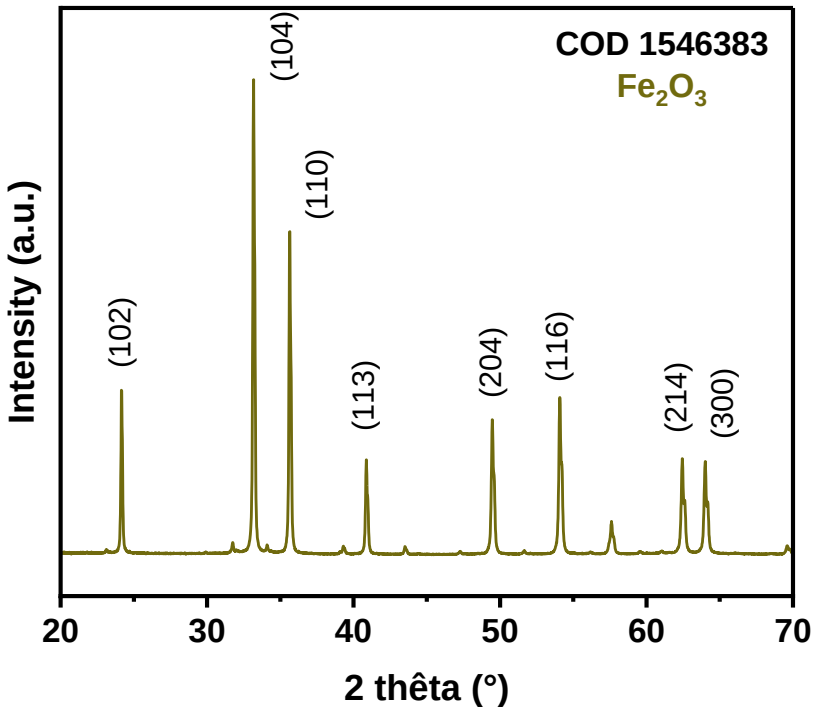

Figure S 5: XRD diffractogram of TGA residue under air at 900 °C for C/FeS_2 A 4h

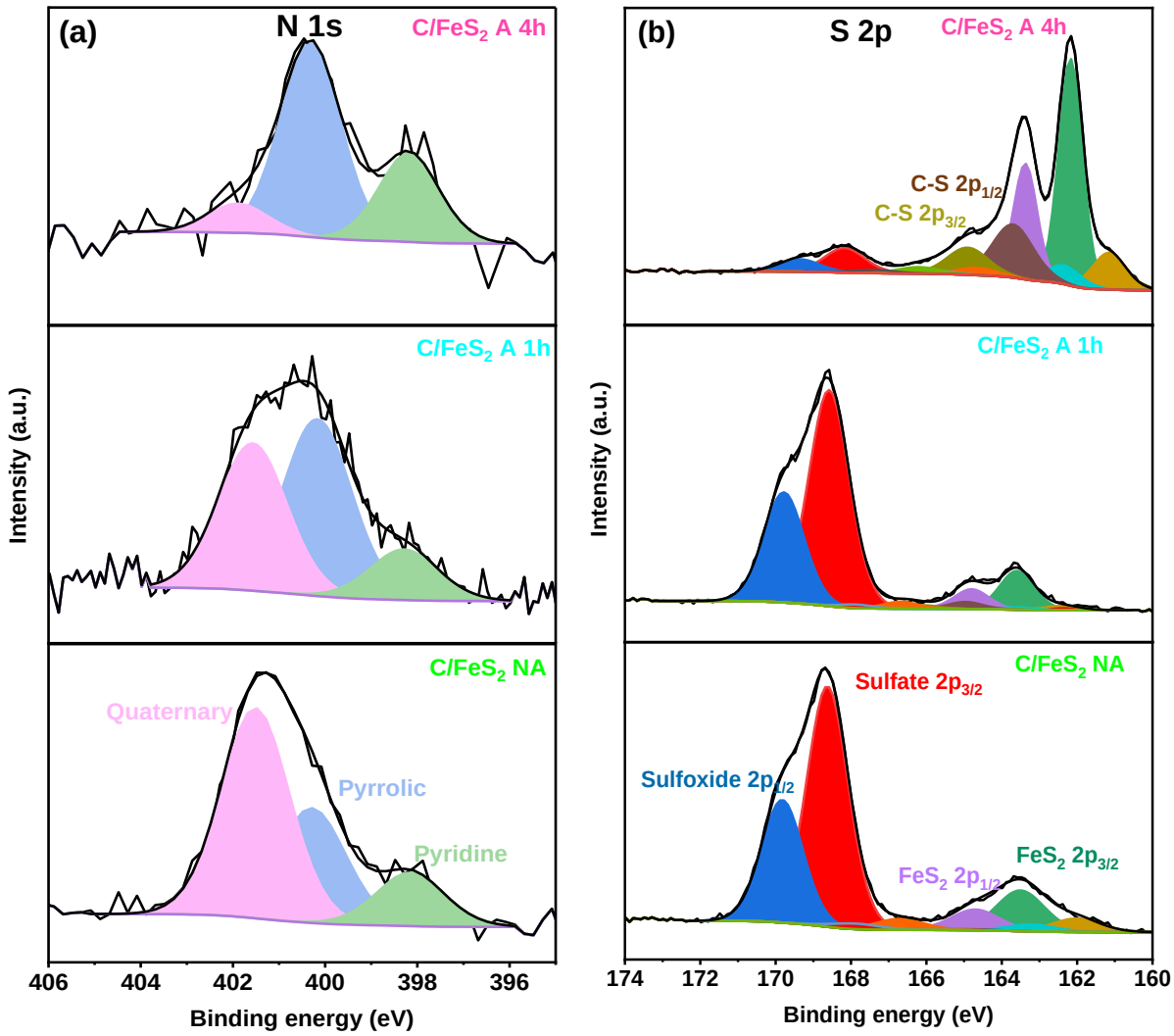

Figure S 6: High resolution deconvoluted XPS spectra of (a) nitrogen, N1s and (b) sulfur, S2p for C/FeS_2 NA, C/FeS_2 A 1h, C/FeS_2 A 4h.

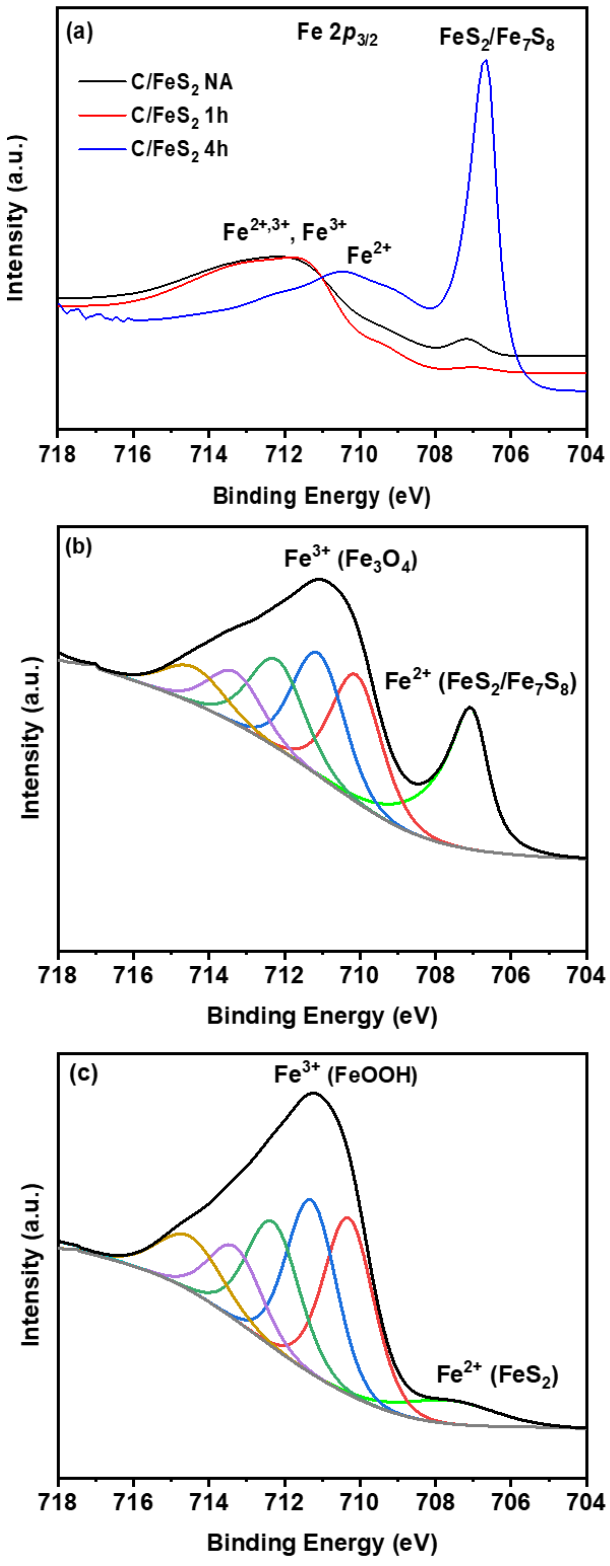

Figure S 7: Comparison of Fe 2$p_{3/2}$ XPS spectra of (a) C/FeS_2 NA, C/FeS_2 A 1h and C/FeS_2 A 4h and high resolution deconvoluted Fe 2 $p_{3/2}$ XPS spectra of (b) C/FeS_2 A 4 h pristine electrode and (c) the same electrode after 50 cycles performed in KOH in a 3-electrode system.

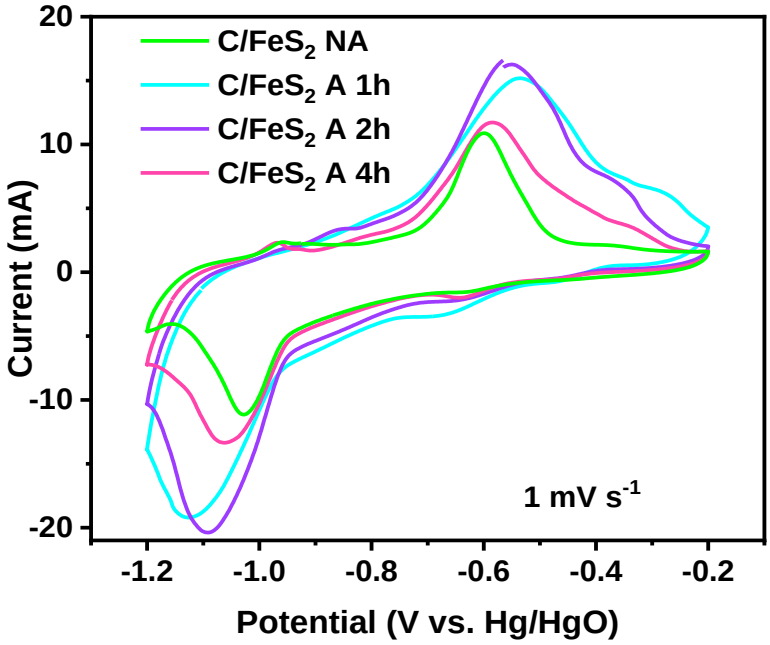

Figure S 8: Cyclic voltammetry (cycle 51) at 1 mV s^{-1} in three-electrode cell using 2 M KOH electrolyte and C/FeS_2 composites.

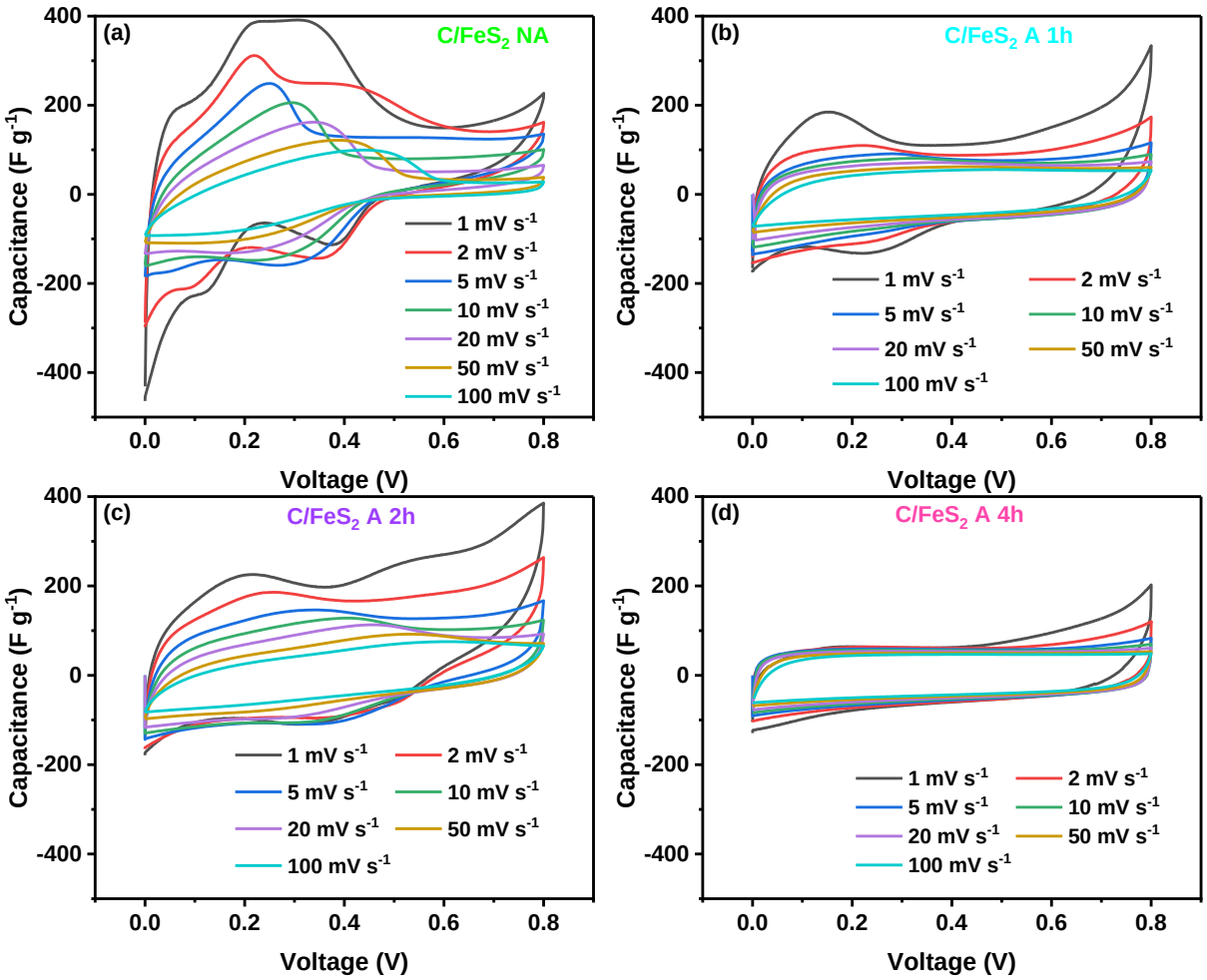

Figure S 9: CV in symmetric 2-electrode cell using 2 M KOH as electrolyte for (a) C/FeS_2 NA (b) C/FeS_2 A 1h, (c) C/FeS_2 A 2h and (d) C/FeS_2 A 4h.

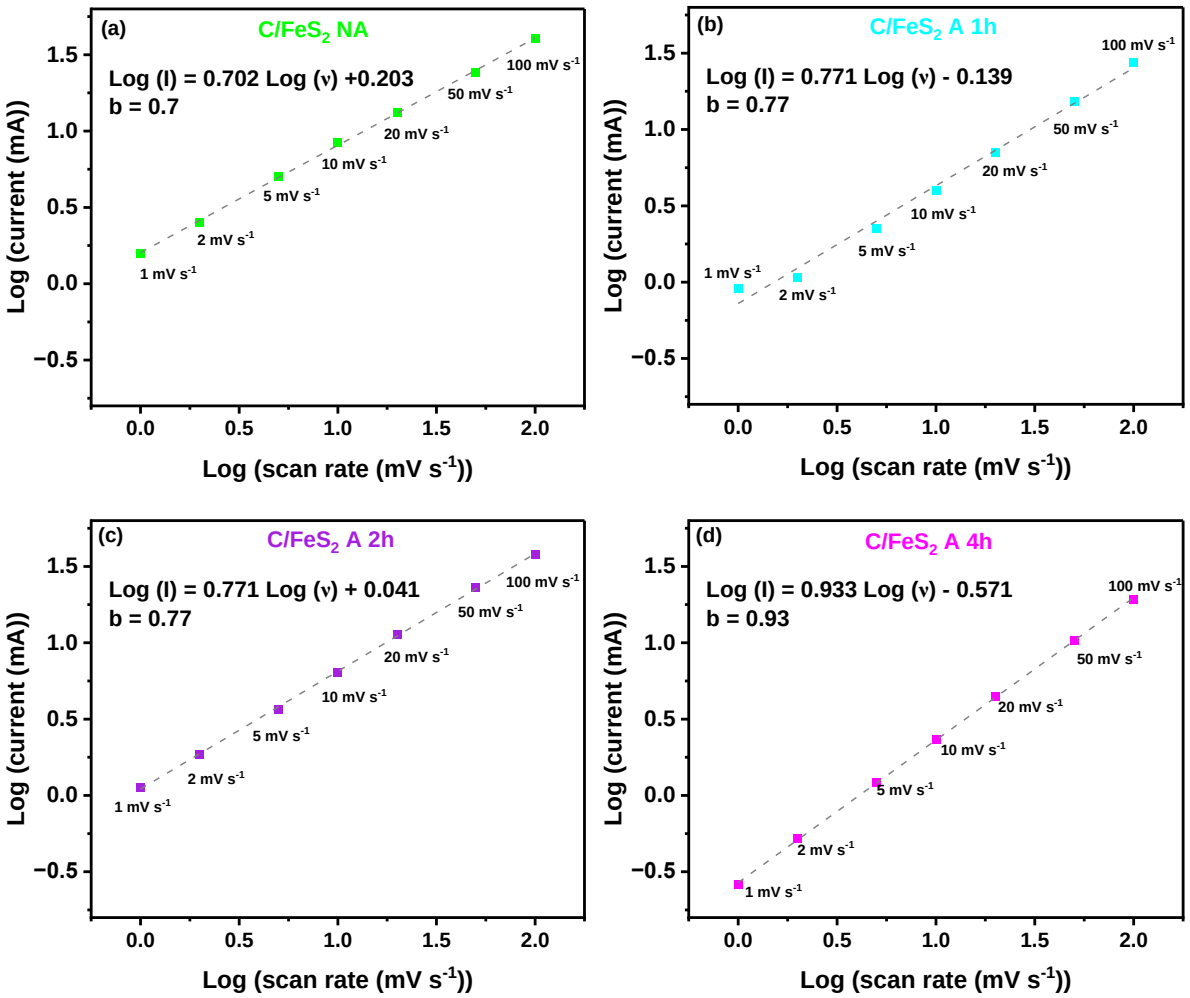

Figure S 10: The correlation of peak current with scan rate in 2 electrode cell for (a) C/FeS_2 NA (b) C/FeS_2 A 1h (c) C/FeS_2 A 2h (d) C/FeS_2 A 4h.

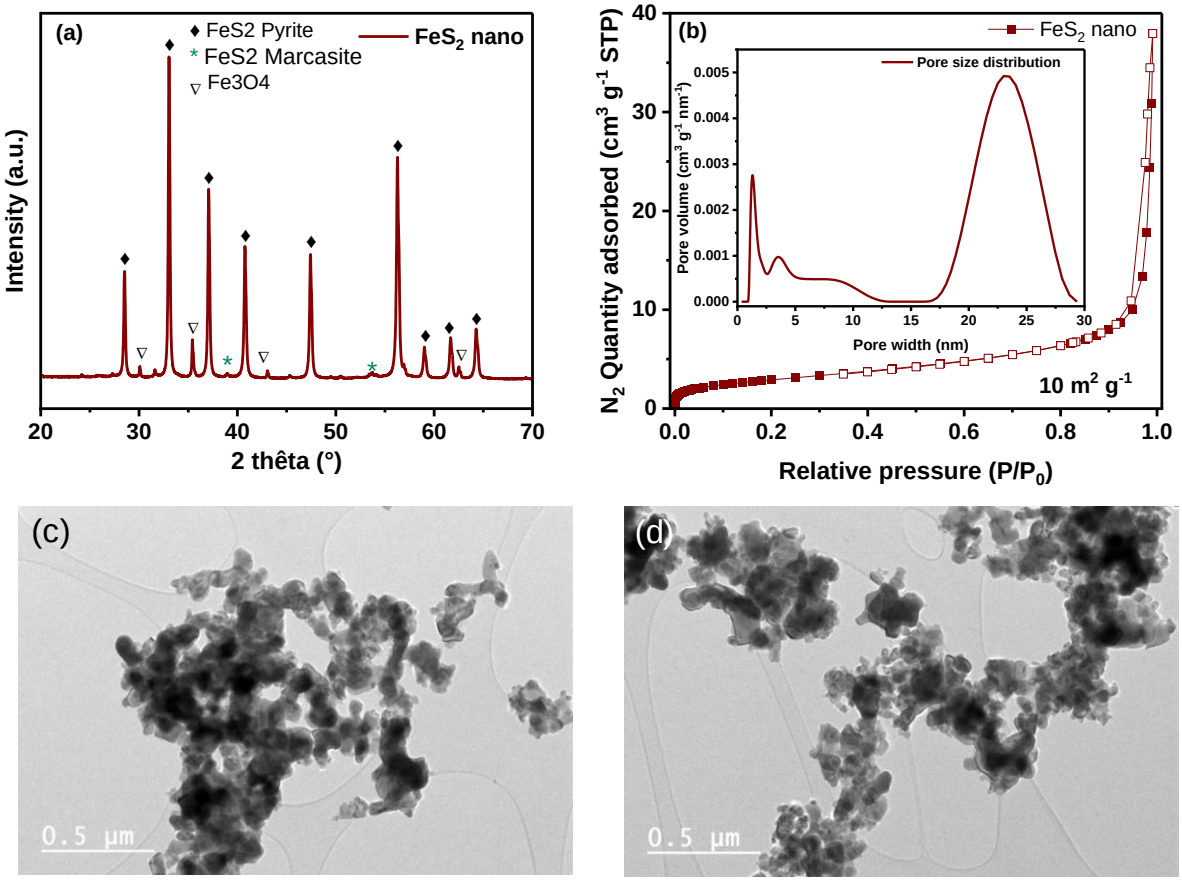

Figure S 11: Nano-FeS_2 main characterization: (a) XRD patterns, (b) N_2 adsorption isotherm, *inset*: pore size distribution from 0 to 30 nm determined by 2D-NLDFT model and, (c,d) TEM image with 0.5 µm scale.

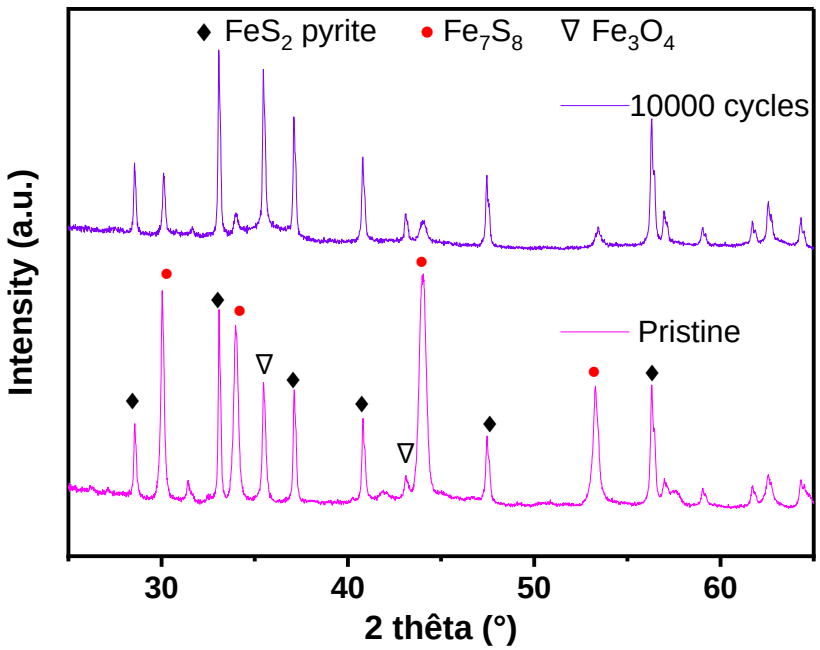

Figure S 12: XRD diffractograms of C/FeS_2 A 4h before and after long cycling for 10000 cycles.

Table S 1: Comparison of the electrochemical performance (specific capacitance and long cycling) of the results obtained in this work (2 electrode cell) with reported literature works (3-electrode cells) on FeS_2 composites for supercapacitors

Material	Type of cell	Electrolyte	Voltage window V	Specific capacitance F g^{-1} at current density A g^{-1}	Retention at long cycling	Ref
FeS_2/3D-porous carbon	Solid state supercapacitor	PVA-KOH	1.8	254 at 2	84,8 after 5000 at 2 A g^{-1}	[2]
FeS_2/carbon nanofibers	3 electrode cell	30 wt% KOH	1.2	406 at 1	97% after 2000	[3]
FeS_2/graphene aerogel	3 electrode cell	6 M KOH	0.7	313 at 0.5	88.2 after 2000 at 10 A g^{-1}	[4]
FeS_2/carbon nanospheres	3 electrode cell	1 M KOH	0.9	278 at 1	57.7% after 10000 at 5 A g^{-1}	[5]
FeS_2/N-S-doped graphene	3 electrode cell	6 M KOH	0.6	528 at 1	89.9 after 10000 at 10 A g^{-1}	[6]
FeS_2/N-S-doped mesoporous carbon	Symmetric 2 electrode cell	2 M KOH	0.8	59 at 0.1	132% after 10000 at 1 A g^{-1}	This work

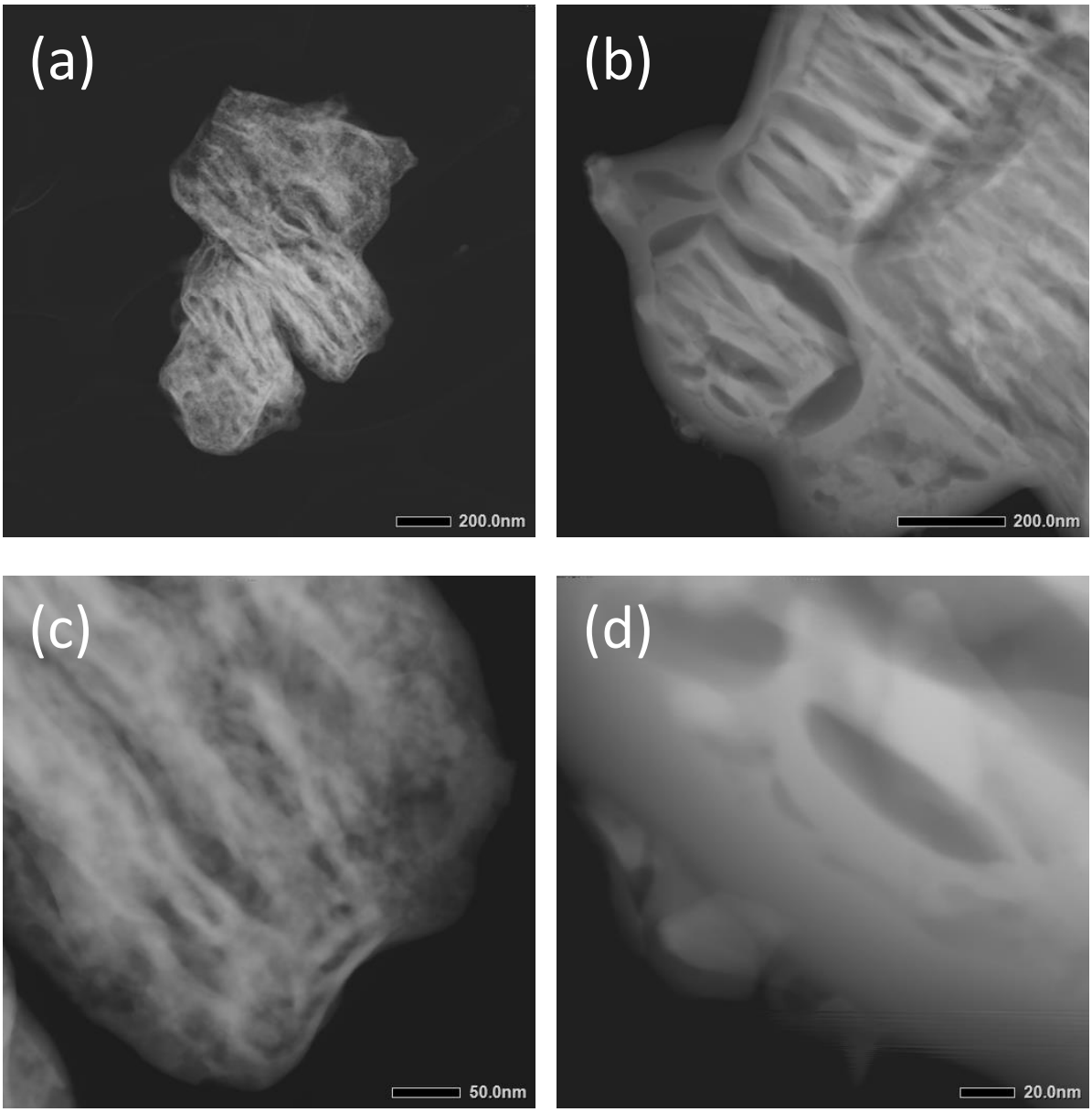

Figure S 13: STEM image of C/FeS_2 NA after 110 days of evolution in ambient conditions (atmosphere and temperature) at different scales (200 to 20 nm).

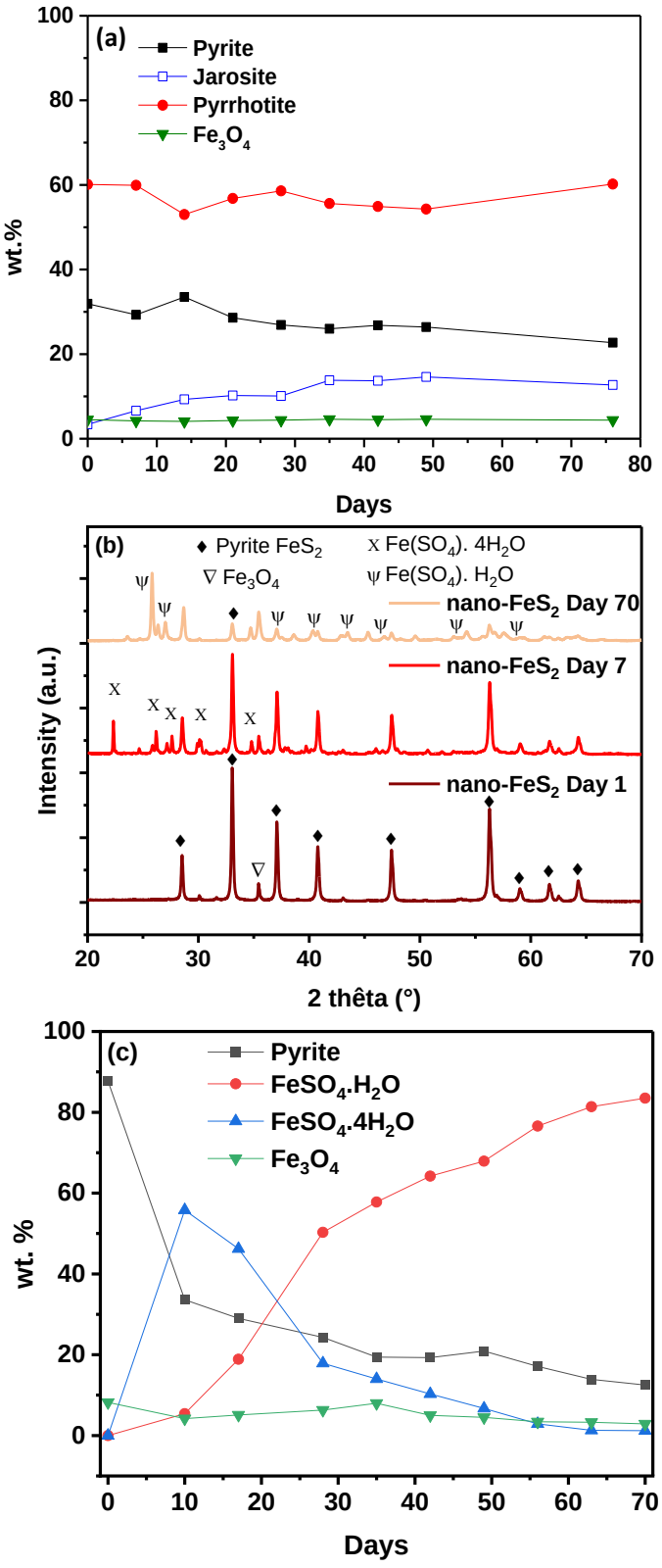

Figure S 14: (a) semi-quantitative analysis with approximate percentage of present crystalline phases in C/FeS_2 A 4h materials at different time scales in days (b) XRD data of FeS_2 nano at day 1 and day 7 (c) and semi-quantitative analysis with approximate percentage of present crystalline phases in nano-FeS_2 materials at different time scales in days.

References:

[1] S. Gražulis, D. Chateigner, R.T. Downs, A.F.T. Yokochi, M. Quirós, L. Lutterotti, E. Manakova, J. Butkus, P. Moeck, A. Le Bail, J Appl Cryst 42 (2009) 726–729.

[2] Y. Huang, S. Bao, Y. Yin, J. Lu, Applied Surface Science 565 (2021) 150538.

[3] V. Sridhar, H. Park, Journal of Alloys and Compounds 732 (2018) 799–805.

[4] L. Pei, Y. Yang, H. Chu, J. Shen, M. Ye, Ceramics International 42 (2016) 5053–5061.

[5] X. Liu, W. Deng, L. Liu, Y. Wang, C. Huang, Z. Wang, New Journal of Chemistry 46 (2022) 11212–11219.

[6] Y. Wang, M. Zhang, T. Ma, D. Pan, Y. Li, J. Xie, S. Shao, Materials Letters 218 (2018) 10–13.